SYSTEMS BIOLOGY

Spatiotemporal NF-κB dynamics encodes the position, amplitude, and duration of local immune inputs

Minjun Son[1,2], Tino Frank[3], Thomas Holst-Hansen[4], Andrew G. Wang[1], Michael Junkin[1,3], Sara S. Kashaf[1], Ala Trusina[4], Savaş Tay[1,2]*

Infected cells communicate through secreted signaling molecules like cytokines, which carry information about pathogens. How differences in cytokine secretion affect inflammatory signaling over space and how responding cells decode information from propagating cytokines are not understood. By computationally and experimentally studying NF-κB dynamics in cocultures of signal-sending cells (macrophages) and signal-receiving cells (fibroblasts), we find that cytokine signals are transmitted by wave-like propagation of NF-κB activity and create well-defined activation zones in responding cells. NF-κB dynamics in responding cells can simultaneously encode information about cytokine dose, duration, and distance to the cytokine source. Spatially resolved transcriptional analysis reveals that responding cells transmit local cytokine information to distance-specific proinflammatory gene expression patterns, creating "gene expression zones." Despite single-cell variability, the size and duration of the signaling zone are tightly controlled by the macrophage secretion profile. Our results highlight how macrophages tune cytokine secretion to control signal transmission distance and how inflammatory signaling interprets these signals in space and time.

INTRODUCTION

Response to infection requires cellular coordination in a wide range of temporal and spatial scales. The innate immune response starts with pathogen detection by sentinel cells like macrophages, which coordinate gene expression in nearby cells through secreted cytokines. Propagating cytokine signals relay information about the type, severity, timing, and location of pathogen inputs. Signaling pathways like nuclear factor κB (NF-κB) play a vital role in interpreting such signals (*1*). Signals from self (cytokines or chemokines) and from pathogens (bacterial or viral components) both activate NF-κB transcription factors, which rapidly shuttle into the cell nucleus and lead to expression of signal-specific response genes.

Previous studies showed that the temporal characteristics of NF-κB are key for immune regulation, and dysfunction of NF-κB dynamics is associated with diverse pathologies from autoimmune disorders to cancer (*2*, *3*). Extensive study of single-cell NF-κB dynamics resulted in improved mechanistic insight in pathway activation and control of signal-specific gene expression and led to the development of accurate computational models of immune gene regulation (*4*–*6*). However, NF-κB signaling in a spatial context has not been studied in detail, and the cellular and molecular mechanisms behind spatial coordination of cells during innate immune response are not clear.

Immune cells must coordinate local and global tissue-level responses at various spatial scales (*7*, *8*). Theoretical studies predicted that cytokine signals create a sharply defined cell activation zone in tissue (*9*, *10*), while a recent in vivo study showed that size of the signaling range depends on the density of cytokine-consuming cells (*11*). Despite these earlier works, studies addressing spatiotemporal aspects of signaling are rare, mainly due to the difficulties in tracking dynamic processes between cells. Quantitative understanding of spatiotemporal cellular communication could lead to broadly applicable models on the emergence and progression of infection, immunity, and autoimmunity and can lead to developing effective therapies (*12*–*14*).

Several questions on spatial regulation of immune signaling are outstanding. First, cellular responses are naturally variable and subject to molecular noise. For example, cytokine secretion from individual macrophages shows different concentrations and temporal changes under identical pathogen inputs (*15*–*17*). Furthermore, signal-receiving cells like fibroblasts respond to cytokines in a highly variable manner (*6*, *18*, *19*). How single-cell variability affects information transfer, signaling range, and gene expression at various distances from the infection site is not understood.

In addition, it is not known whether signaling networks can determine distance and location of the signal source in tissue. The dose and duration of a cytokine signal provide information about the severity and persistence of the pathogen load in the tissue microenvironment. Secreted cytokines form concentration gradients, which could enable responding cells to locate the pathogen input. However, simultaneously determining the dose and location of a cytokine input is challenging because high dose in gradient could indicate either proximity to the source or a high initial cytokine release. Thus, measurement of the dose alone may not provide enough information to the cells about the severity and location of the pathogen input.

While it is not clear whether signaling networks are capable of simultaneously decoding pathogen load and location, the dynamical characteristics of NF-κB provide potential for such multidimensional information processing (*20*, *21*). The time course of a local cytokine signal depends on initial cytokine release and distance, and NF-κB dynamics in single cells is highly sensitive to such changes (*22*). This suggests the intriguing possibility that NF-κB may simultaneously decode the amplitude, duration, and location of a pathogen input. Determining the spatiotemporal processing abilities of signaling pathways would greatly improve our understanding of how immune cells spatially coordinate their inflammatory responses.

To study how localized cytokine signals control NF-κB signaling and gene expression in space and time, we developed a microfluidic

[1]Pritzker School of Molecular Engineering, University of Chicago, Chicago, IL 60637, USA. [2]Institute for Genomics and Systems Biology, University of Chicago, Chicago, IL 60637, USA. [3]Department of Biosystems Science and Engineering, ETH Zürich, Basel 4058, Switzerland. [4]Niels Bohr Institute, University of Copenhagen, Copenhagen 2100, Denmark.
*Corresponding author. Email: tays@uchicago.edu

coculture system that mimics conditions during inflammatory signaling after infection (Fig. 1C). Using this system and mathematical modeling, we investigated how pathogen detection by macrophages is broadcast to nearby cells and how these signals are interpreted by the NF-κB network in individual cells at different locations. Through computational simulations and live-cell analysis, we found that the signaling range and duration are highly variable and depend strictly on the rate of cytokine production by macrophages. Unexpectedly, we find that the NF-κB network can simultaneously measure the dose, duration, and distance of a cytokine signal, despite the variability in the signal-receiving cell population. Spatially resolved gene expression measurements showed that cells convert spatially varying signals into distinct spatial gene expression patterns within the responding cell population, creating "gene expression zones." Our studies established a computational model of NF-κB signaling in space and time and revealed how the NF-κB and inflammatory signaling networks extract complex information from their environments under pathogen infection.

RESULTS

We computationally and experimentally considered a localized infection scenario that creates a one-way communication channel from a signal-sending macrophage to signal-receiving fibroblasts (Fig. 1A). First, pathogen molecules [bacterial lipopolysaccharide (LPS)] activate a macrophage in the infection site. The macrophage releases tumor necrosis factor (TNF) that diffuses to neighboring cells and activate the NF-κB pathway. NF-κB regulates gene expression in a spatially and temporally varying manner in the responding population. We primarily focused on TNF signaling, as prior work showed that TNF is the main secreted factor from the RAW macrophages used in this study (*23*). This result was further confirmed by measuring the cytokine secretions from these cells (fig. S1). Upon stimulation by LPS, macrophages rapidly secreted TNF increasing by almost 100-fold, compared to less than fourfold for all other measured cytokines. Furthermore, fibroblasts used in this study do not release signaling factors that activate NF-κB in other cells (fig. S5). This ensures that the communication scenario that we created is one way, from the macrophage to the fibroblast population.

Spatiotemporal modeling of NF-κB activity in a one-way communication scenario

To theoretically study spatial NF-κB signaling in our infection scenario, we built a simple model where TNF is released from a point source and allowed to diffuse freely through a long chamber filled with signal-receiving cells (Fig. 1C). The response of each cell was simulated according to an ordinary differential equation model of NF-κB dynamics in response to TNF (Fig. 1B). To capture how variable activation affects signaling, each cell was assigned a random activation threshold [normal distribution, covariance (CV) = 0.2]. This spatiotemporal mathematical model allowed us to probe how local TNF release produces a spatially and temporally resolved NF-κB response in a neighboring cell population (Fig. 1, F and G, and figs. S2 and S3).

Our modeling studies presented two interesting observations: the presence of a well-defined NF-κB activation zone in the responding population, and wave-like propagation of NF-κB activation. Despite single-cell activation variability, a well-defined NF-κB activation zone was created in the responding population, with a narrow boundary region between activated and nonresponsive cell populations (Fig. 1F). Within this zone, NF-κB activity spread in a wave-like manner, where a band of NF-κB activation propagated away from the TNF source (Fig. 1G).

Microfluidic experiments show a defined activation zone and wave-like NF-κB propagation in response to a cytokine source

To experimentally study spatiotemporal NF-κB response to local cytokine release, we developed a microfluidic device that can precisely control cytokine release from an isolated (source) chamber (Fig. 1C) (*23*). To activate fibroblast cells, either soluble TNF or a single macrophage is first loaded in the source chamber. Then, a polydimethylsiloxane (PDMS) membrane valve is opened to allow the soluble TNF or macrophage secretions to diffuse into a receiving chamber filled with fibroblast cells (Fig. 1D and movie S1). The bottom end of the receiving chamber was continuously replenished (flowed) with fresh medium to simulate the role of capillaries in supplying fresh nutrients and depleting cytokine signals by providing a sink effect (*24*). Our device thus simulates a localized infection and subsequent innate immune signaling scenario in tissue.

To track NF-κB response at the single-cell level, we used 3T3 mouse embryonic fibroblasts expressing NF-κB fusion reporter (p65-dsRed). Fluorescence images reporting NF-κB nuclear localization were captured every 6 min and then analyzed with custom image analysis program to quantify NF-κB response in individual cell (*25*–*27*).

Our live-cell imaging experiments supported the qualitative predictions from our mathematical model. When TNF was released from the source chamber, fibroblast population showed wave-like propagation of NF-κB activation in the receiving chamber (Fig. 1H and movie S2). Receiving cells were exposed to different cytokine kinetics depending on their distance to the signal source (Fig. 1E). Cells at farther distance experienced slower increase in TNF concentration and lower maximal dose (fig. S4), which also delayed the onset of NF-κB activation (purple interval in Fig. 1I) and extended the activation time (blue interval in Fig. 1I) (*6*, *22*). When these shifts are coupled with the oscillatory characteristics of the NF-κB network, it prompts a robust wave-like spread of NF-κB activation in the responding population.

Wave-like propagation could theoretically be due to signal secretion and amplification by responding cells (*28*, *29*). However, when we stimulated a subpopulation of fibroblasts with TNF, nearby fibroblasts did not show NF-κB activation, indicating that these cells do not secrete NF-κB–activating signals (fig. S5). Thus, our results indicate that diffusion of TNF coupled with intrinsic features of the NF-κB network is sufficient to produce wave-like activation in the receiving cell population.

Our experiments also reproduced the sharply defined activation zone predicted by simulations (Fig. 1J). For all tested source doses, the activation rate of receiving cells transitioned from >75 to <25% in less than 0.4-mm distance (<15% of the chamber length). Furthermore, the signaling range (defined as a distance where 50% of regional cells are activated) varied minimally between culture replicates with the same source dose. These results indicate that the NF-κB signaling range is precisely defined, despite variable single-cell activation inherent to the NF-κB network (*6*). These findings motivated us to study how the signaling range is affected by different cytokine secretion patterns from the source.

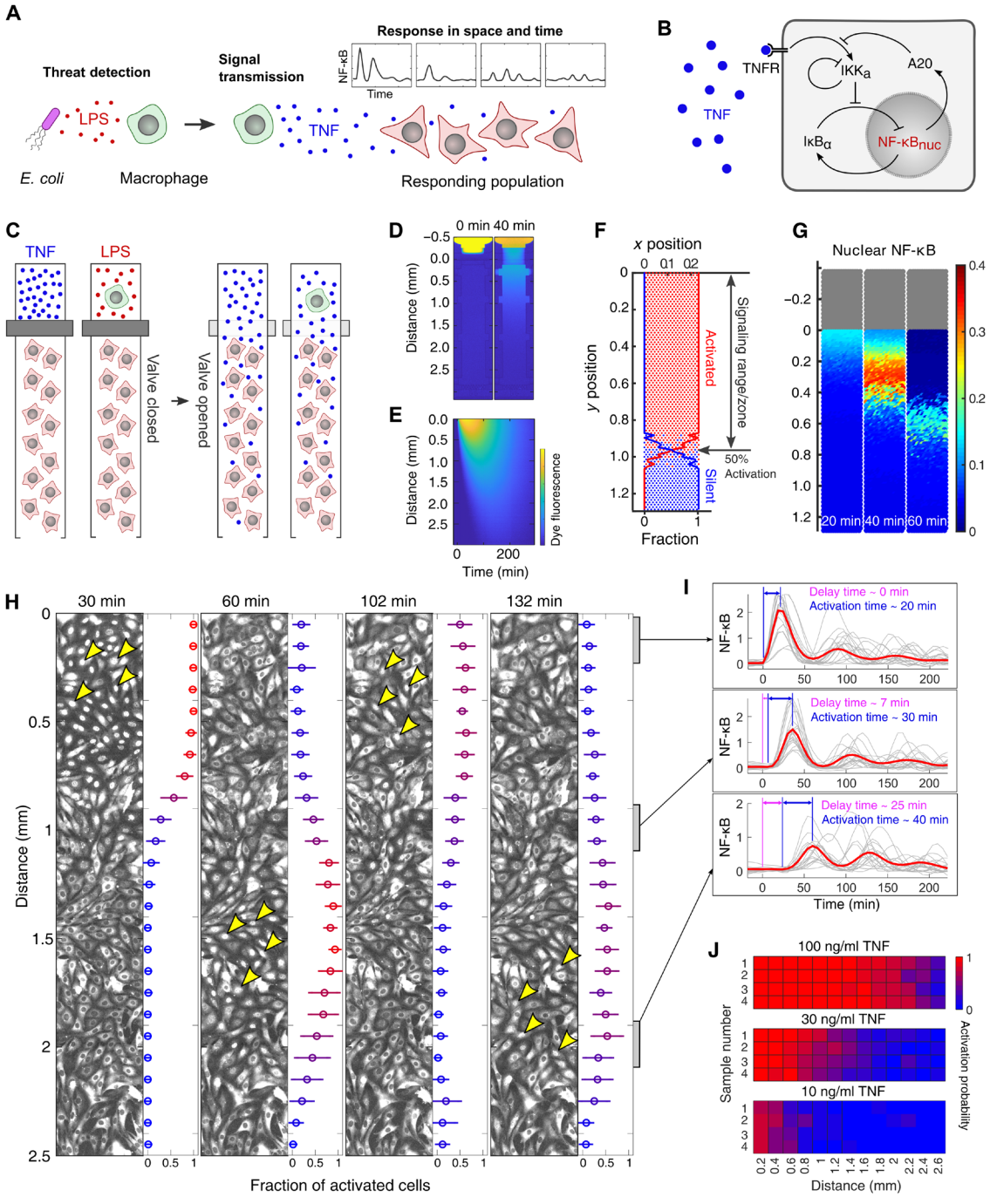

Fig. 1. Cytokine secretion from a local source induces wave-like NF-κB propagation and a finite cell activation zone. (**A**) Diagram illustrating a model of immune signaling following a local infectious signal. (**B**) Simplified NF-κB network for mathematical modeling. TNFR, tumor necrosis factor receptor. (**C**) Microfluidic device designed to study the infection scenario in (A). Either TNF or a single macrophage was loaded in the source chamber. The macrophage was stimulated with LPS and washed with fresh medium. When the valve is opened, TNF or macrophage secretions diffuse into receiving chamber. (**D**) Diffusion of signals in the receiving chamber tested with fluorescent dye. (**E**) Heatmap shows kinetics of dye fluorescence over distance. (**F**) NF-κB activation at each location derived from simulation. Cell activation probability was calculated at various distance from source. Each point represents a single cell with the regulatory network in (B). (**G**) Simulation shows the release of TNF from source chamber elicits wave-like NF-κB propagation in receiving population. (**H**) Microfluidic experiments exhibited wave propagation of NF-κB activation after release of TNF (100 ng/ml) from the source chamber. Fluorescently tagged NF-κB shuttles into the nucleus upon activation. Yellow arrow heads indicate examples of activated cells. Bar graphs on the right illustrate the fraction of activated cells at different distances. Circles and error bars indicate the mean and SD in 10 replicates. (**I**) NF-κB responses in near (0 to 0.4 mm), mid (0.8 to 1.2 mm), and far (1.8 to 2.2 mm) regions. Red lines show the mean of all responses in each region ($n > 300$), while gray lines represent 20 random responses. Purple indicates the delay time between the initiation of TNF diffusion and onset of NF-κB activation, while blue indicates the activation time. (**J**) Activation probability at various distance for three different TNF doses. Each dose had four replicates.

Dose and duration of a cytokine signal independently control the range of signaling and number of NF-κB oscillations in receiving cells

Cytokine secretion from immune cells reflects the information about cell type, its current state, and the severity of the infectious challenge (*16*, *30*, *31*). Different secretion patterns can potentially affect NF-κB signaling range and dynamics in receiving cells. In particular, previous studies demonstrated that a high number of NF-κB oscillations preferentially induce genes that determine cell fate and cause epigenetic remodeling through expression of late-term target genes (*4*, *6*). Thus, we investigated how particular cytokine release parameters (e.g., dose and duration) affect the signaling range and NF-κB dynamics in nearby cells.

Returning to mathematical modeling, we adjusted the dose and duration of cytokine secretion from a point source and evaluated how secretion pattern affects the spatial NF-κB response (Fig. 2, A and B). Our simulation suggests that spatial features of NF-κB response to the same amount of cytokine depend primarily on the rate of release. Slow TNF secretion (Fig. 2B, red) resulted in a short signaling range (distance from source) but a high number of NF-κB oscillations within the range. On the other hand, fast TNF secretion (Fig. 2B, blue) showed long signaling range but low number of oscillations. When we only varied the dose of TNF secretion while keeping the duration constant, the signaling range linearly correlated with the logarithm of the source dose, but the number of oscillations was not affected (Fig. 2C). On the other hand, the number of NF-κB oscillations correlated to the duration of TNF release but was independent of the dose. Varying source dose did not affect the number of NF-κB oscillations, nor did varying duration affect the signaling range. Thus, our results indicate that dose and duration are two independent aspects of cytokine release that control different parameters of NF-κB response in signal-receiving cells.

We experimentally tested these predictions using our microfluidic system. When various doses of TNF (10, 30, or 100 ng/ml) were released from the source chamber, the signaling range increased proportionally to the logarithm of the source dose (Fig. 3, A and C). Similarly, when the TNF stimulus was released for different durations (15, 30, and 60 min), the number of NF-κB oscillations in the activation zone increased at longer stimulus durations (Fig. 3, B and C, and fig. S6). Regardless of the release duration, we observed a similar signaling range, with only ~10% increase in the range between 15 and 60 min. However, we observed a small increase in the number

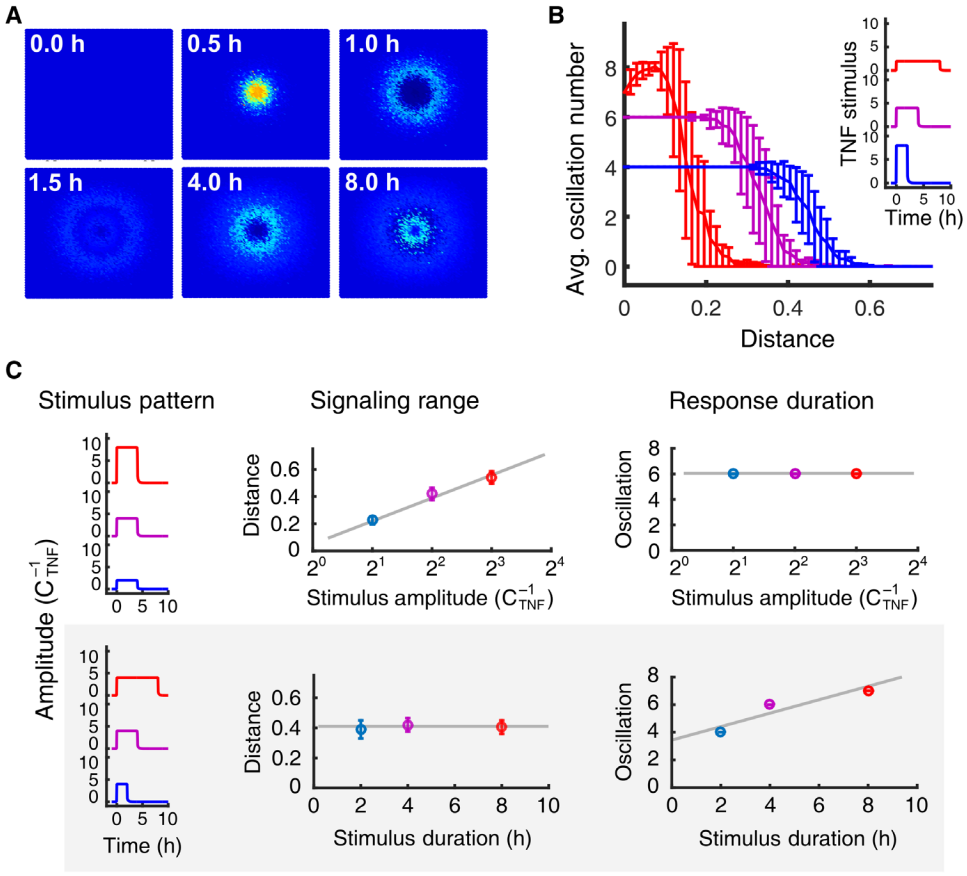

Fig. 2. Modeling predicts that cytokine secretion dose and duration controls NF-κB response in distinctive and independent manner. (**A**) NF-κB activation in a two-dimensional (2D) tissue is simulated in response to TNF release at the center. (**B**) Spatiotemporal NF-κB responses to different secretion profiles with varied amplitude and duration are simulated. The total amount of cytokine or area under the curve (AUC) in each profile is fixed for comparison. Blue indicates the population response for short and high release, while red indicates the response for long and low release. (**C**) From simulated results, the effect of secretion amplitude and duration on signaling range and number of oscillations is evaluated. Secretion profiles (stimulus pattern) and corresponding responses (signaling range and response duration) are grouped by color. Between the top and bottom panels, the same color indicates stimuli with the same AUC.

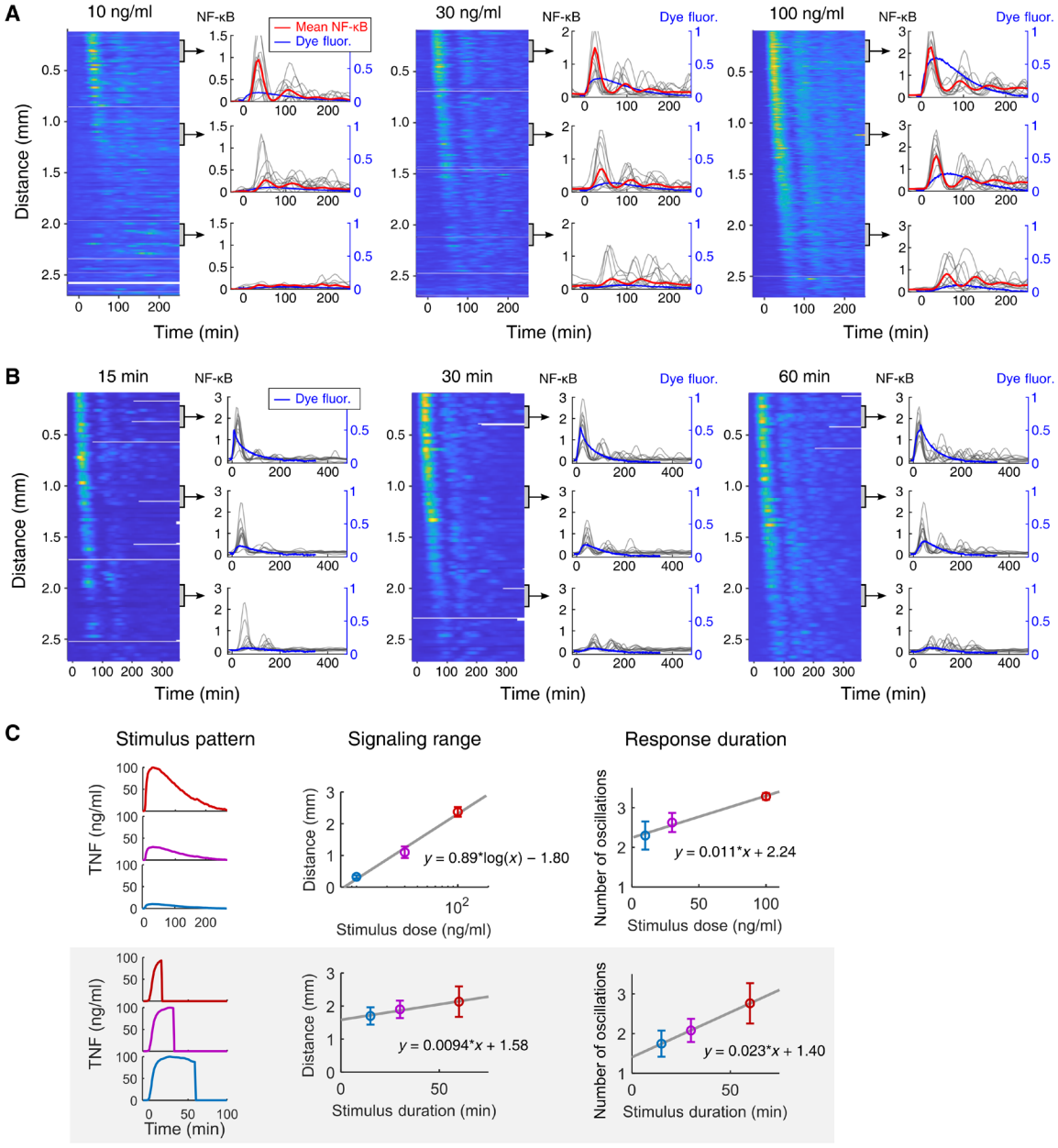

Fig. 3. Dose and duration of cytokine secretion independently control the NF-κB signaling range and number of oscillations, respectively. (**A** and **B**) Heatmaps and traces depict the spatiotemporal NF-κB response to the TNF release from a source. Experiments were conducted with three different doses of TNF (10, 30, or 100 ng/ml) or by closing the separating valve 15, 30, or 60 min after releasing TNF (100 ng/ml). The plot on the right shows the NF-κB behavior in three different regions (top, mid, and bottom) in the cell chamber. Red lines show the mean behavior, while thin gray lines show 10 random dynamics in each region. Blue lines show TNF dynamics predicted from the dye diffusion in Fig. 1D. (**C**) Similar to Fig. 2C, the effect of different stimulus patterns on the signaling range and number of oscillations is evaluated using the experimental data from (A) and (B). Stimulus patterns are adapted from the diffusion test with fluorescent dye (Fig. 1, D and E). Data in signaling range and response duration are displayed as means ± SD from three replicates.

of oscillations depending on the source dose, despite our computational prediction that the two are independent (Fig. 3C). This disagreement could be due to experimental depletion of TNF in the source chamber (stimulus patterns in top panel of Fig. 3C), unlike the pulsatile stimulus used in our simulation. Regardless, we note that the number of oscillations was over twice as dependent on stimulus duration compared to stimulus dose. Overall, our simulation and experiments demonstrate that the signaling range strictly depends on the dose of stimulus, while the number of oscillations depends significantly more on the duration of the stimulus.

NF-κB independently decodes the dose, duration, and distance of a cytokine source

We investigated whether the NF-κB dynamics in signal-receiving cells can independently decode the three key features of the signal source: the initial dose and duration of cytokine secretion and its

distance. First, to study how NF-κB dynamics change over distance, we organized the measured single-cell responses based on their distance to the source chamber (figs. S7 to S8). As noted earlier, some differences, such as higher first peak or faster activation for closer cells, were due to the cytokine gradient formed by diffusion along the receiving chamber (Fig. 1C). However, we also observed that other parameters, such as the height and width of later peaks and the number of oscillations, significantly varied in a manner that cannot be attributed to the gradient alone (Fig. 3A and figs. S3 and S9 to S11). In particular, cells located closer to the source had narrower and higher initial peaks followed by sharply decreased second peaks, while cells located farther had lower initial peaks but stronger second peaks.

To examine whether these differences in the first and second peaks are sufficient to identify cell's distance to the cytokine source, we quantified the peak heights and area under the curve (AUC) from each cell and clustered cells based on similarity in these parameters [Fig. 4, A and B; see fig. S12 for TNF dose (30 ng/ml)]. When the cell positions in each cluster were plotted, we found that cells in each cluster were located at a similar distance from the TNF source (Fig. 4C and fig. S12). The single-cell distances in each cluster were significantly different from the distances in the other clusters (fig. S13).

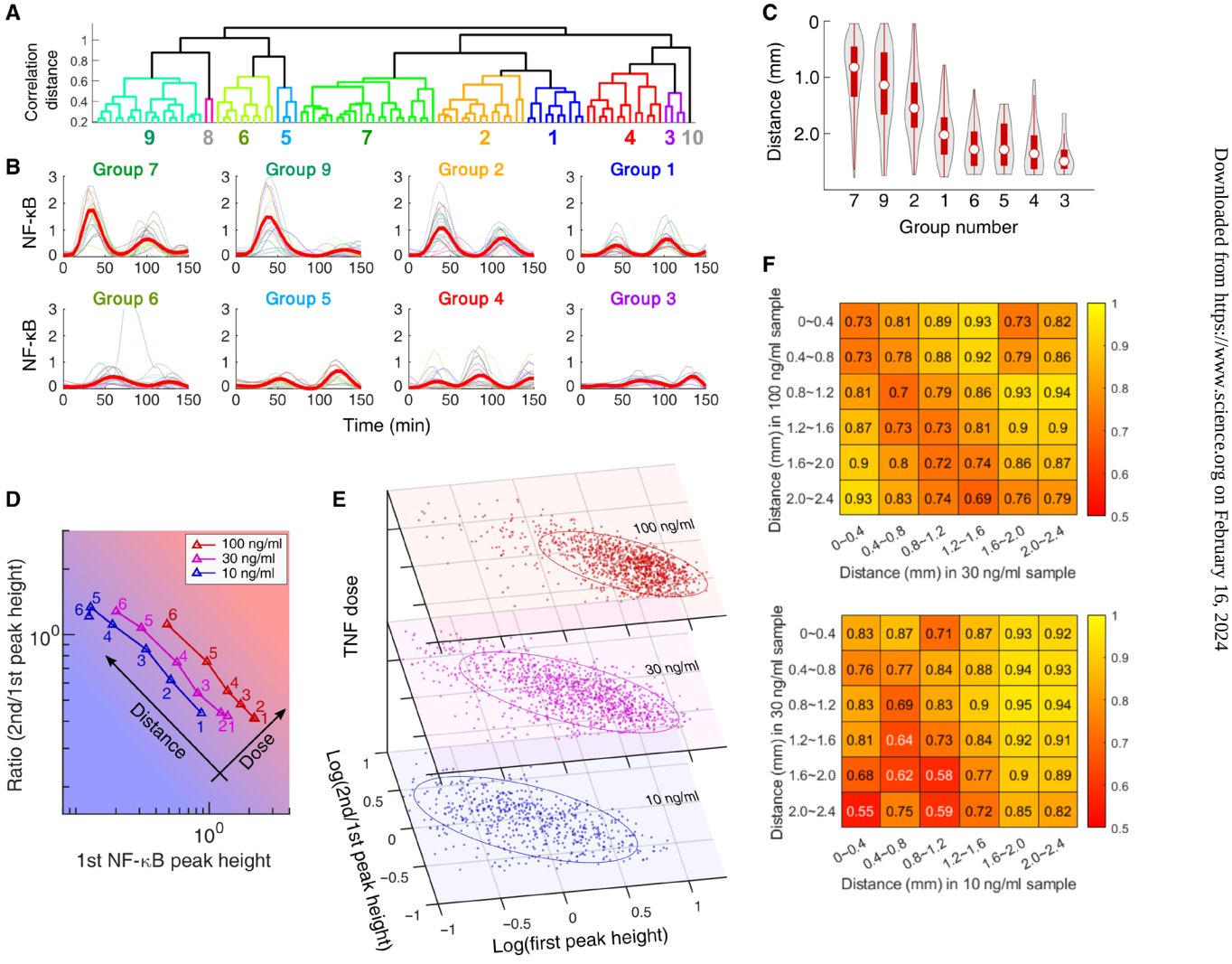

Fig. 4. Dose, duration, and location of the cytokine source can be simultaneously determined from the NF-κB dynamics in the receiving cells. (**A**) Dendrogram shows the NF-κB dynamics in response to source dose (100 ng/ml) divided into 10 clusters. For each cell, the height and AUC of the first two peaks are quantified and used as input for clustering. (**B**) Subplots show the NF-κB response behavior in eight major clusters. Thin lines show 20 random cell traces. Subplots were arranged on the basis of the distance from the TNF source. (**C**) Violin plots quantifying the spatial distribution of cells in each cluster. Red boxes indicate 25 and 75 percentiles, while circles represent the median distance. See fig. S13 for the statistical comparison. (**D**) Triangles show the mean first peak height and the mean ratio between the first and second peak heights at six different distances from the cytokine source. Number on each point represents the relative distance to the source with one being closest. (**E**) Single-cell data from different source doses are plotted in the same format as in (D). The ellipses indicate 20% quantile isoline. (**F**) The single-cell accuracy in distinguishing source dose and location is evaluated through cross-validation of the decision tree. The numbers in heatmaps indicate the distinguishability between the single-cell responses in two locations from different source doses. Here, 1 indicates total distinguishability, while 0.5 indicates total indistinguishability.

Thus, the peak height and width within NF-κB dynamics contain enough information to define the receiving cell's distance to the signaling source.

We then examined whether the source cytokine dose can be also identified from the NF-κB dynamics alone. Comparison of the dynamics at the same distance from different source doses shows that the height of the first peak increased with the source dose (Fig. 3A). In contrast, the ratio between the first two peak heights specifically depended on the cell's distance to the cytokine source. Irrespective of source dose, the ratio of the second peak height to first peak height increased with distance from the cytokine source (fig. S14). This result still held true when AUC of the peaks were compared instead of peak heights (fig. S14). Thus, a simple comparison of dynamic NF-κB features can elucidate two distinct attributes of the signaling source over distance.

Plotting the mean height of the first peak against the ratio between the first two peaks revealed that cells from different distances line up along a single trajectory (Fig. 4, D and E, and fig. S15). When single-cell traces from different source doses were analyzed and plotted together, each dose formed distinct and parallel trajectories, implying that each distance and source dose can be differentiated from every other distance and source dose. Therefore, the cytokine dose and distance from the signaling source can be quantified independently, solely from the heights and ratio between the first two NF-κB peaks. In the previous section, we showed that the number of NF-κB oscillations in the receiving cells corresponds to the duration of the cytokine release. Therefore, our analyses collectively indicate that, if there are more than two oscillations present in the NF-κB dynamics, then the dynamics contain sufficient information to simultaneously distinguish the dose, duration, and location of the cytokine source.

Although we find that the population mean of NF-κB dynamics carries multidimensional information about a cytokine source, the single-cell responses vary significantly (Fig. 4E and figs. S7 to S11). To evaluate how accurately NF-κB dynamics estimate the location, dose, and duration of a cytokine stimulus in single cells, we classified single-cell responses using binary decision trees. NF-κB localization traces from each source dose and duration were aligned on the basis of the onset timing of activation (figs. S16 and S17A) and were divided into six or five groups on the basis of their distance to the cytokine source. The accuracy of distinguishing between each group was quantified using 10-fold cross-validation (Fig. 4F for different dose and fig. S17B for duration). For example, the number in the top left corner of the heatmap shows the distinguishability between the responses in first positions of two samples, where 1 indicates perfect distinguishability and 0.5 indicates total indistinguishability. Between the samples (30 and 100 ng/ml), groups were readily distinguished at the single-cell level (Fig. 4F). All cells were classified with an accuracy of 0.69 to 0.94, even between the groups exposed to similar amount of cytokines, e.g., positions 4 and 5 with a source dose of 100 ng/ml versus positions 3 and 4 with a source dose of 30 ng/ml (fig. S4). The distinction between groups still persisted when we compared cells from conditions with lower source doses, although the accuracy dropped to 0.55 to 0.94 due to higher relative noise at lower doses. For the comparison between different TNF secretion durations, we observed similar classification accuracy ranging from 0.53 to 0.92 (fig. S17B). However, we also notice significantly different patterns between heatmaps from different source dose and different source duration classification. Unlike the different source dose, most of the low distinguishability in different duration comes from comparing samples from the same distances (i.e., the diagonal entries in heatmaps), indicating the variance in the second or further NF-κB oscillation is substantial enough to undermine the small change in the secretion duration. However, we highlight that this low probability is improved when samples with larger difference in secretion duration are compared (15 min versus 60 min in fig. S17B), showing that the different number of oscillations can still play an important role in distinguishing the secretion duration. Overall, despite noise in the NF-κB network, our analysis shows that individual cells can, in theory, process the local cytokine dynamics and decode information about cytokine secretion dose, duration, and its relative location.

Macrophage secretion variability determines NF-κB signaling range and duration

TNF secretion by macrophages varies significantly between individual cells even under identical pathogen stimuli (*16*, *32*), but the consequence of cytokine variability on NF-κB signaling is not understood. To predict the effect of variable cytokine secretion on NF-κB signaling range, we used previously measured TNF secretion profiles from single macrophages as input to our stochastic model simulations (Fig. 5A) (*16*). We found little variation in the signaling range (the physical extent of NF-κB activity in the responding cell population) when the same secretion profile was tested multiple times, despite variability in the NF-κB response of receiving cells (Fig. 5A, top). However, using different secretion profiles from macrophages resulted in highly variable signaling range (Fig. 5A, bottom). Thus, the difference in cytokine secretion dynamics is readily translated into variation in the NF-κB activation range.

To validate this prediction, we performed macrophage-fibroblast coculture experiments that modeled inflammatory signaling from an activated macrophage to neighboring fibroblasts. A single RAW264.7 macrophage was loaded into each source chamber in our coculture device, stimulated with LPS (50 ng/ml) for 10 min, and washed with fresh medium to remove LPS. The separator valve was then opened to allow LPS-induced macrophage secretions to diffuse to fibroblast population (Fig. 1B). This stimulation method induced strong NF-κB activation in most macrophages, although the duration of NF-κB activation varied widely (1 to 4 hours) in each macrophage (Fig. 5B). In addition, by removing LPS, we could strictly monitor how the variance in the cytokine secretion from macrophage affects the signaling over distance without the influence from LPS.

The coculture experiments also showed wave-like propagation of NF-κB activation through the receiving cells (Fig. 5B and movie S3), similar to our observations from TNF diffusion experiments (Fig. 1G). However, unlike TNF diffusion experiments, we observed a wide range of signaling distances and durations when activated macrophages were used as signal source (Fig. 5C and fig. S18). Our experiment with 35 samples, each with a single macrophage in the source chamber and 100 to 200 fibroblasts in the receiving chamber, showed that the NF-κB signaling range varied from almost 0 to 2 mm. Likewise, the number of NF-κB oscillations in the receiving cells varied from 0 to more than 3, depending on each macrophage and location of the receiving cell (Fig. 5C and fig. S18). Compared to the minimal variation that we found from earlier TNF diffusion experiments, different secretion patterns by macrophages had a significant influence on the signaling range and number of NF-κB oscillations in the surrounding cells. Thus, our results suggest that the local macrophage secretion patterns tune and directly control the local inflammatory response during infection.

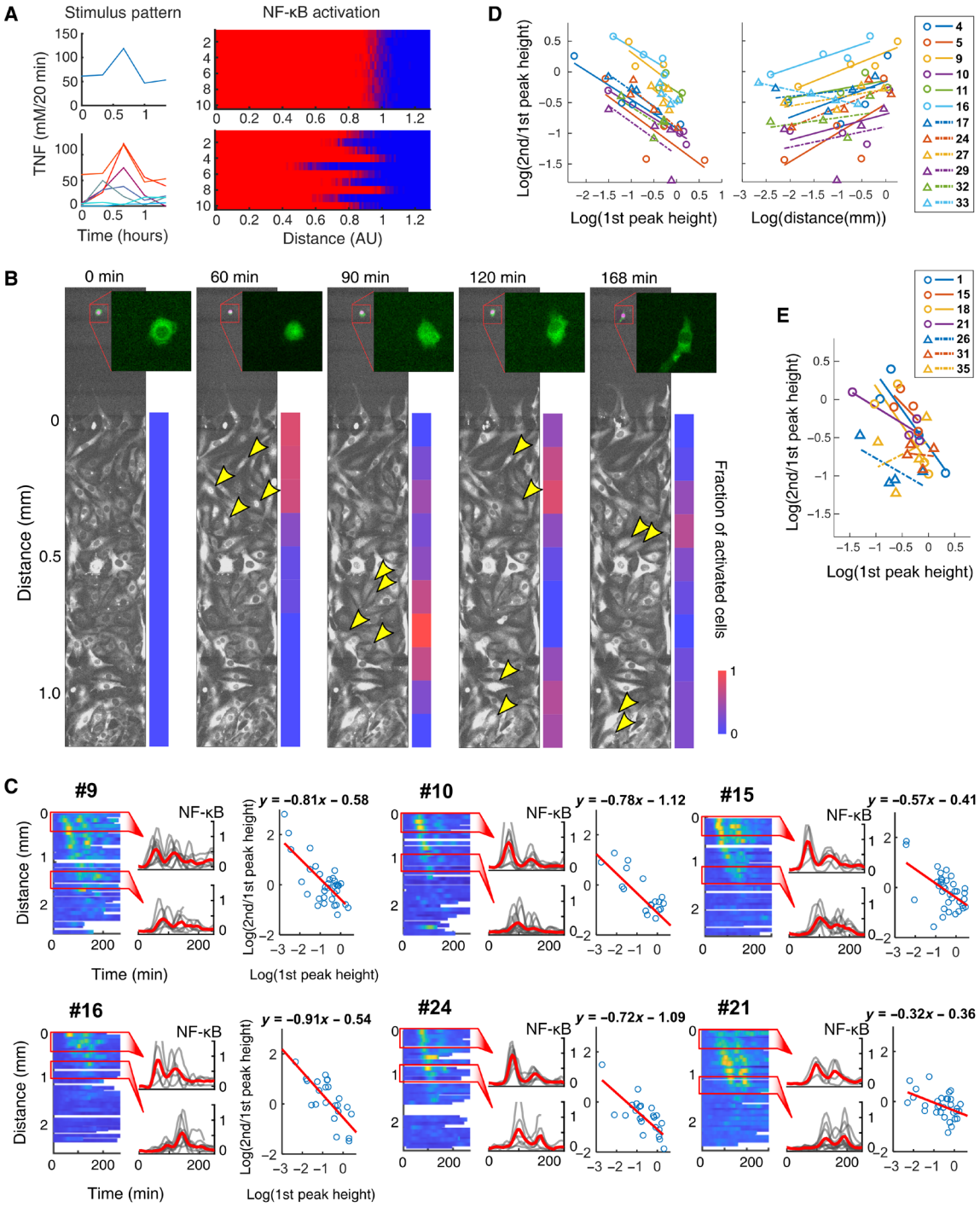

Fig. 5. Macrophage cytokine secretion dictates the signaling range and duration. (**A**) Using measured TNF secretion profiles from macrophage, the effect of stochastic NF-κB response on signaling range is simulated. Top right shows the results from 10 different trials using an identical secretion profile (top left). Bottom right shows the results from each secretion profile shown on the left. (**B**) Time lapse fluorescence images show our coculture experiments, which imitate the tissue infection. A macrophage harboring p65-gfp was stimulated with LPS (10 ng/ml; green cell in the inset), which released TNF to activate NF-κB in the receiving population (bottom chamber). Yellow arrow heads indicate examples of activated cells in each microscopy image. The color bar on the right shows the activation rate at various distance. (**C**) Heatmaps and single-cell traces show six examples of the spatiotemporal NF-κB response induced by single macrophages. The scatter plot on the right shows the single-cell data and fitted line similar to Fig. 4 (D and E). See fig. S18 for all samples. (**D** and **E**) Similar to Fig. 4D, the receiving chamber is divided into four different regions, and the median ratio between the first and second peaks and the median first peak height in each region are quantified (symbols in the plot). For each sample, the best-fit line through those four data points is calculated and overlaid on the same plot. In addition, the relationship between distance and peak ratio is also compared. Numbers in the legend correspond to the numbers in (C) and fig. S18. Samples with similar slopes (CV < 0.33, calculated from the best-fit lines in the left plot) are shown in (D), while outliers are shown in (E).

We also highlight that the NF-κB pathway in fibroblasts was able to decode the cytokine dose and distance to the macrophage despite the variability in the secretion patterns. When the ratio between the first and second NF-κB peaks was plotted against distance or against first peak height, roughly 60% of trajectories had similar slopes (slope CV < 0.33; Fig. 5D and #9, #10, #16, and #24 in Fig. 5C). While a minority of experiments displayed aberrant NF-κB dynamics (Fig. 5E and #15 and #21 in Fig. 5C), most of the samples behaved similarly. Hence, despite variability in single macrophages, NF-κB dynamics retain the ability to encode the receiving cell's relative location and the dose of cytokine secretion from macrophage.

Cytokine dynamics determines spatial gene expression patterns in the responding population

Although we demonstrated that the NF-κB dynamics in receiving cells can encode the distance and dose of the secreting source (Fig. 4), how these differences in dynamics affect the transcription of response genes is unclear. Previous studies suggest that mRNA degradation rate is a key parameter in understanding different kinetics of NF-κB target genes (*6*, *22*, *33*, *34*). Genes involved in NF-κB feedback, like the inhibitor of nuclear factor κB (IκB) family and A20, are not only rapidly expressed upon TNF stimulus but also rapidly degraded (early genes). On the other hand, inflammatory response genes, e.g., those related to apoptosis or chemokine signaling, show slower activation and prolonged expression afterward (late genes). We hypothesized that each NF-κB target gene would show a distinct expression pattern over the activation zone, depending on its dynamic characteristics and the responding cell's distance to the cytokine source.

To estimate how local gene expression profiles change at different distances from the signaling source, we added a simple gene expression component to our mathematical model and varied the degradation rate of mRNA (Fig. 6A and Materials and Methods). Early genes closely followed NF-κB localization dynamics, rapidly diminishing upon NF-κB inactivation. As a result, expression of early genes is restricted to the vicinity of the source, where NF-κB oscillations persisted for longer time. On the other hand, late genes slowly accumulated during NF-κB activation and remained high even after NF-κB inactivation. When the duration of stimulus was long enough, the difference in gene expression characteristics resulted in a spatial pattern, where early genes were up-regulated in vicinity of the cytokine source while late genes rose at longer distances.

We tested this prediction by measuring gene expression from three different regions in the receiving chamber in TNF diffusion experiments (Fig. 6B). Using a custom microfluidic device, cells were retrieved from all three regions (and at multiple time points: 0, 2, 4, and 8 hours) following exposure to the spatial gradient formed by a source dose of 100 ng/ml. Reverse transcription quantitative polymerase chain reaction (RT-qPCR) was used to measure the kinetics of key early and late NF-κB response genes in the responding population from each three locations (Fig. 6C) (*6*). Early genes (*A20*) were rapidly induced and degraded, while late genes (*Casp4/RANTES*) rose and fell more slowly. These trends led to spatial patterning of gene levels at later time intervals. At 8 hours, *A20* remained highly expressed near the source but sharply decreased at farther distances. In contrast, *Casp4* and *RANTES* were highly expressed in all three regions (near, mid, and far). Combined, our experiments showed spatial patterning of early and late response genes in the responding population, whose distinctive expression profiles are correlated to the NF-κB dynamics and the gene-specific degradation rates.

Spatially resolved RNA sequencing shows distinct proinflammatory gene clusters at different distances from the cytokine source

RNA sequencing was used to more closely investigate the spatial variability in the gene expression patterns. Cells were stimulated with two different source doses (TNF, 30 and 100 ng/ml) and retrieved after 4 hours, where expression levels were close to the maximum for all three genes in our time course measurement (Fig. 6C). Among all genes evaluated, 1094 genes were significantly up-regulated compared to the control (no exposure to TNF) and used for further analysis.

First, to see whether the expression of response genes is differentiated by the receiving cell's location and source dose, we calculated the pairwise distances between the samples and visualized them with multidimensional scaling (MDS; Fig. 6D) (*35*, *36*). In the scatter plot, we noticed that samples were grouped on the basis of the source dose. In particular, the mid and far samples (in source dose of 100 ng/ml) were separated from the near samples (in source dose of 30 ng/ml), although the maximum cytokine concentrations that they experienced during the experiment were similar (fig. S4). To study the correlation between the NF-κB dynamics and downstream gene responses, we sorted the 451 genes, which contain a motif for RelA binding (table S1), and then performed the same analysis on these genes, which reproduced the separation of samples based on dose and distance similar to the results using all up-regulated genes (fig. S19A). These results suggest that genes are differentially regulated on the basis of both location and source dose and that NF-κB dynamics likely plays a role in this differential regulation.

We then performed hierarchical clustering to group genes based on their dependence on the source dose and distance and processed each group through gene ontology (GO) analysis to analyze the functional characteristics of each gene cluster (Fig. 6E and tables S2 to S13) (*37*, *38*). Clustering resulted in six groups with different patterns of up-regulation. In particular, cluster 1 (blue) genes were strongly induced at most distances in both source doses, cluster 2 (red) genes were expressed specifically in the top position of 30 ng/ml, cluster 3 (yellow) genes were strongly expressed in the source dose of 100 ng/ml but not in the source dose of 30 ng/ml, and cluster 4 (purple) included genes that showed strong dependence on position and dose. The GO term analysis shows that clusters 1, 3, and 4 are enriched with genes related to the immune or stress response, which is expected from TNF stimulus. However, genes in cluster 1 were enriched with motifs for interferon regulatory factor (IRF) binding, namely, for motifs related to IRF-1, IRF-2, IRF-7, IRF-8, and IRF-9. In contrast, genes in cluster 4 were enriched with motifs for NF-κB family transcription factors, namely, RelA, p50, and NF-κB2. Because motif analysis does not directly demonstrate which transcription factors associate with the known genes, we turned to existing transcription factor immunoprecipitation databases to compare transcription factor association with clusters 1 and 4 (Fig. 6F). Using the ENCODE database of chromatin immunoprecipitation sequencing (ChIP-seq) results (*39*), we found that a number of transcription factors were enriched in both clusters 1 and 4, including immunity- and inflammation-related transcription factors like signal transducers and activators of transcription 1 (STAT1) and STAT2 (*40*). As we saw with the motif analysis, however, cluster 1 genes were enriched for binding by IRF-1 and IRF-4, while cluster 4 genes were enriched for binding by RelA, suggesting that these clusters are regulated by IRF-1/4 and RelA respectively.

Because genes in cluster 1 were strongly up-regulated in most positions, this result suggests that IRF-1– and IRF-4–dependent genes

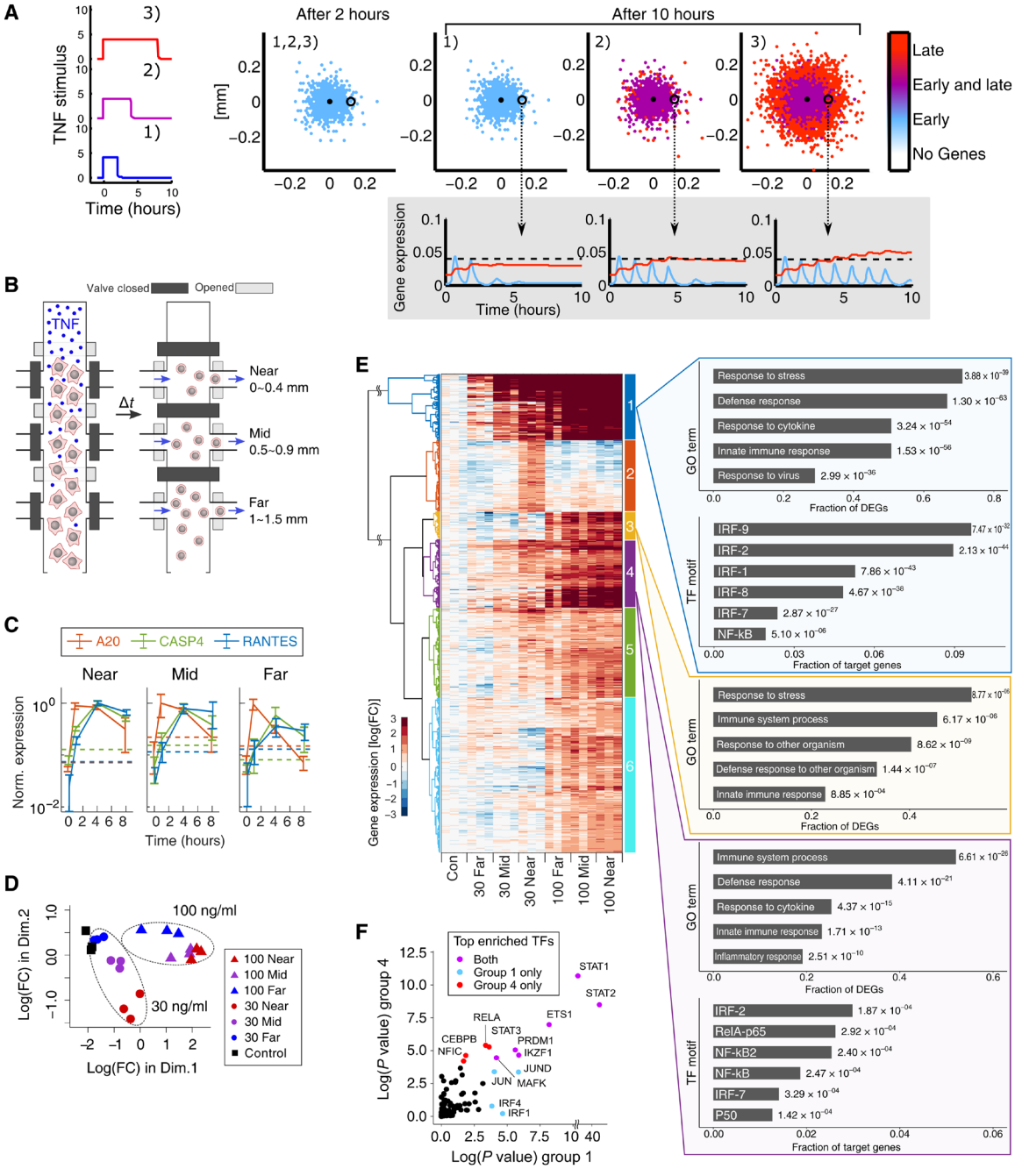

Fig. 6. Spatially resolved gene expression analyses highlight distinct proinflammatory gene clusters depending on distance and source dose. (**A**) Downstream expression from three different cytokine secretion durations (2, 4, and 8 hours) are simulated with our 2D model. At each point, the corresponding NF-κB dynamics are input to the gene expression function. Blue indicates genes with rapid degradation (early), while red represents slow degradation (late). Gene activation is determined by whether the expression has reached a threshold (0.05) during the simulation (10 hours). (**B**) Diagram illustrates the schematics of spatially resolved downstream measurement using a custom microfluidic chip. (**C**) Cells from three different regions are collected at 0, 2, 4, and 8 hours after releasing TNF (100 ng/ml) from source chamber. Then, using reverse transcription quantitative polymerase chain reaction (RT-qPCR), the expression of A20 (early), CASP4, and RANTES (late) genes is measured. Error bars show SD from three replicates. Each gene is normalized to its highest mean level among all conditions. The dashed lines indicate the three SDs above the mean before stimulation. FC, fold change. (**D**) Cells from different regions are collected 4 hours after releasing TNF of 30 or 100 ng/ml. After sequencing, the pairwise distance between samples is compared in the MDS plot for 1094 significantly up-regulated genes. (**E**) Up-regulated genes from sequencing data are clustered using correlation method. The functional characteristics of genes in each cluster were analyzed through enrichment of GO terms and TF (transcription factor) motifs. The numbers on the right indicate the *P* value. (**F**) The scatter plot compares enrichment of TF binding in group 1 versus group 4. The enrichment is calculated from ENCODE TF ChIP-Seq database using ChEA3. For each group, the top 10 enriched TFs are colored on the basis of whether they are enriched in group 1 (blue), group 4 (red), or both groups (purple).

are highly sensitive to TNF stimulus and can drive long-range effects during inflammatory signaling. In contrast, NF-κB–dependent genes were mostly up-regulated close to the source, possibly due to the higher threshold for activation by TNF (Fig. 7). Thus, the difference between IRF-1 and IRF-4 target gene expression and NF-κB target gene expression would increase at farther distances, producing spatial variability in inflammatory gene expression patterns. Because IRF-1 signaling is induced by NF-κB and acts as a modulator of NF-κB signaling, it raises the possibility that IRF-1 actually acts as a sensitive and strong amplifier of NF-κB signaling following TNF stimulus (*41*, *42*). Unexpectedly, some immune genes are almost independent of the distance (cluster 3). Although the maximum cytokine concentration was higher in the near position of 30 ng/ml than the far position of 100 ng/ml (fig. S7), immune genes in cluster 3 were strongly expressed in all positions of 100 ng/ml while hardly expressed in any of 30 ng/ml sample. These data show that dose-dependent but distance-independent signaling is possible within the signaling zone (Fig. 7). The other clusters (clusters 2, 5, and 6) showed up-regulated genes related to cell growth and metabolism as well as stress response (tables S5, S11, and S13). To further investigate whether these diverse expression patterns can be induced by NF-κB target genes, we performed similar hierarchical clustering for the 451 genes containing RelA binding motif and the 86 RelA target genes identified by ChIP-seq (table S14). Although the size of each cluster varied, we observed largely similar clustered groups arise from the selected genes (fig. S19, B and C), suggesting that the different NF-κB dynamics by source dose and distance (Fig. 4) may play significant role in distinct gene regulation in each cluster. Overall, our sequencing analysis demonstrates different roles for two transcription families in inflammatory signaling and classifies immune genes that are regulated on the basis of the distance to the source and/or the source doses.

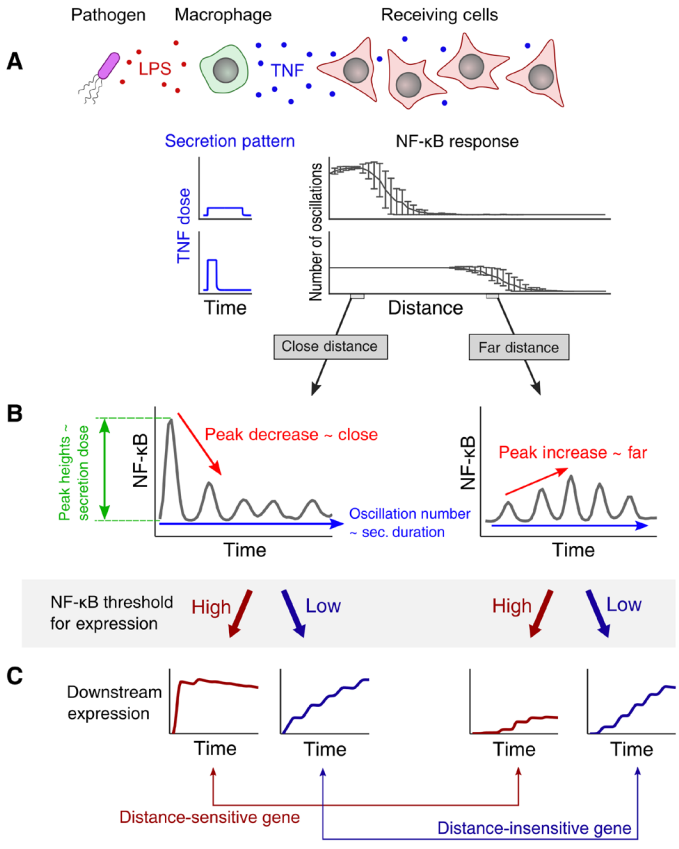

Fig. 7. Cytokine secretion pattern determines NF-κB activation range and duration, and responding cells regulate distance-specific inflammatory responses. (**A**) The dose of cytokine secretion by a macrophage controls signaling range, while the duration of secretion controls the number of oscillations in the responding cells. (**B**) Gray lines represent single-cell NF-κB dynamics at close and far distances, while colored arrows highlight the different features of NF-κB dynamics corresponding to different attributes of cytokine secretion by the macrophage. (**C**) Using the NF-κB dynamics in (B) as input, the kinetics of two downstream genes (red and blue) with different NF-κB thresholds are simulated.

DISCUSSION

Inflammatory signals in response to infection are often initiated from a localized point in the cellular microenvironment. In this study, we used the NF-κB network to explore how localized cytokine secretion affects spatiotemporal aspects of proinflammatory signaling at the single-cell and population levels (Fig. 7A). Through mathematical modeling, microfluidic coculture experiments, and spatially resolved gene expression analysis, we showed that localized cytokine secretion from a macrophage creates wave-like propagation of NF-κB activation in responding population. The range of signal propagation is sharply defined and strictly correlated to the dose of cytokine release, irrespective of the release duration. On the contrary, the number of NF-κB oscillations in the signaling zone depends on the release duration. Hence, the signaling range and duration of NF-κB response in a cell population are two independent properties that can be attributed to dose and duration of cytokine secretion. Stochastic regulation of the NF-κB network minimally affected these properties of spatial response. Hence, each macrophage can tune its cytokine secretion pattern to control the range and duration of the inflammatory response in the neighboring cells. Unexpectedly, NF-κB dynamics can independently encode the dose, duration, and location of a cytokine source (such as a macrophage) and give rise to distinct gene expression patterns depending on the cytokine secretion dose and distance. Overall, our study highlights the ability of the NF-κB signaling network to gain detailed information about a signal source by interpreting the kinetics of diffusing cytokines and to coordinate distance and source-specific responses in a cell population (Figs. 6 and 7, B and C).

RNA sequencing analysis from different locations in the responding cell population revealed a group of immune genes that showed strong correlation to the cytokine dose rather than to distance. Because cytokine secretion dose is correlated with the severity of infection [i.e., the pathogen load (*43*)], this suggests that receiving cells can interpret the severity of infection from the diffusing signal even at a distance. Such a capability would allow local cells to coordinate their inflammatory response based on the distance and severity of the infection to accurately interpret and overcome infectious challenges.

In addition, we found that IRF-family genes (IRF-1, IRF-2, IRF-7, IRF-8, and IRF-9) are more sensitive to TNF than NF-κB–family genes, resulting in a significantly longer signaling range for IRF target genes. These genes are closely associated with antiviral innate immunity, and previous studies have shown its cross-talk with the NF-κB pathway (*44*, *45*). However, IRFs can also control distinct inflammatory pathways (*46*), and recent studies have shown that differential regulation between NF-κB and IRF-7 promotes different inflammatory responses (*47*). Because our analysis showed that the differential

regulation between IRFs and the NF-κB pathway is enhanced at farther distance, these results indicate that different activation thresholds for two distinct transcription factors can be used to fine-tune distance-specific inflammatory responses.

MATERIALS AND METHODS

Cell culture

Mouse fibroblast ($p65^{-/-}$ NIH 3T3) harboring H2B–green fluorescent protein (GFP; nucleus marker) and p65-DsRed (NF-κB marker) was cultivated using Fluorobrite Dulbecco's modified Eagle's medium (DMEM; Gibco, A1896701) supplemented with 10% fetal bovine serum (FBS; Omega Scientific, FB11), 1% GlutaMax (Gibco), and 1× penicillin-streptomycin (Gibco). For passaging, cells were harvested by adding Trypsin-EDTA (Gibco), washed, then resuspended in fresh medium (1:10) before reaching 100% confluency in regular flask. For macrophage ($p65^{-/-}$ RAW 264.7) harboring p65-GFP reporter, we used the same DMEM medium supplemented with 10% certified FBS (Gibco, A3160401), 1% GlutaMax (Gibco), and Hepes (Gibco, 15630106). Before reaching 100% confluency, cells were scraped and resuspended in fresh medium (1:10).

Microfluidic device fabrication

The patterns for our diffusion microfluidic chip were designed with AutoCAD (Autodesk Inc.) and KLayout. To fabricate the relief mold with the design, we followed the standard soft lithography procedure. For the valve regions on the flow layer, we used positive photoresist (MicroChemicals, AZ40XT) with 20 μm thickness. For the other part of the flow layer or control layer with valves, we used negative photoresist (MicroChemicals, SU-8 3025) with 30 or 25 μm thickness, respectively. All photoresists were exposed to 375-nm laser using the maskless aligner (Heidelberg MLA150). For more details about the mold-making protocol, see Gómez-Sjöberg *et al.* (*48*). For PDMS casting, polymer and catalyst for PDMS (Momentive, RTV-615) were mixed in 10:1 ratio. To create a slab of PDMS grooved with control valve pattern, the PDMS mixture was poured over the mold for control layer. For the control layer, 5 to 10 g of mixture was poured on the mold and spun at 2300 rpm for 1 min to create thin (~50-μm) layer of PDMS. Both mixtures were cured overnight at 80°C. The cured PDMS slab and thin layer were treated with oxygen plasma (Harrick, PDC-001) for 30 s and then were aligned using a custom stage with upright microscope. After additional baking overnight, the holes for the control lines and fluid inlets were punched, and then, the chip was bonded to a clean glass slide through oxygen plasma treatment. More details about the fabrication process are described in our previous publication (*25*).

Microfluidic experiment

Using Tygon tubing (ND-100-80) and metal pins, each valve in the control layer was connected to a pneumatic solenoid valve (Festo, 197334). The tubes were prefilled with water to prevent diffusion of gas to the fluid channels. The solenoid valve was controlled electronically, whose exact timing for opening and closing was controlled by custom developed MATLAB interface. Various medium containing cells or ligand was aliquoted in a pressure relief vial and delivered to the microfluidic chambers through PEEK tubing (VICI, TPK.505). The stage of microscope (Nikon Eclipse Ti2) was surrounded by a custom-made box to maintain the temperature at 37°C (Life Imaging Secrvice, Basel), and the microfluidic device was enclosed in a stage-top incubator, which maintained the chip environment with 5% CO_2 and above 98% humidity. More details about the setup and control over the chip were described in our previous publication (*25*).

For the fibroblast loading, the surface in microfluidic chambers was treated with 1:4 fibronectin (1 mg/ml) in phosphate-buffered saline (PBS) solution overnight and washed with fresh medium, and then, fibroblasts were loaded in the diffusion chamber at about 80% confluency. After seeding, we waited at least 5 hours with one or two feedings in the middle to allow cells to attach and spread uniformly in the diffusion chamber. In the meantime, cells stuck or settled in the other channels were removed by flushing with trypsin. For the macrophage loading in the source chamber, cells were diluted in the fresh medium, and the channel was opened and closed repeatedly until one cell was seated in the source chamber. All microfluidic chips were controlled by a custom graphic user interface (MATLAB), which is a modified version of the previous hardware-software interface developed by Gómez-Sjöberg *et al.* (*48*). The software could also run a prewritten code that automatically feeds, sinks, and purges the microfluidic chambers at designated time.

During the diffusion experiment, the bottom channel of the diffusion chamber was continuously washed by flowing fresh medium through on-chip peristaltic pumping. To ensure consistent cytokine sinking without disturbing the medium inside the diffusion chamber, the peristaltic pumping was performed at very low frequency (0.33 Hz or 20 cycles per minute), and the bypass was washed every 1 to 2 min. This process also allowed the medium exchange by diffusion from the sink to the diffusion chamber and enabled cells to continuously grow without additional feeding. For the diffusion experiment with cytokine, TNF of either 10, 30, or 100 ng/ml (R&D Systems, 410-MT) was loaded in the source chamber, and then, the separating valve was opened, while the bottom sink channel was continuously pumped with fresh medium. For the diffusion experiments with different duration of TNF release (Fig. 3B), TNF (100 ng/ml) was loaded in the source chamber, and the separating valve was opened and then closed after 15, 30, or 60 min. For the coculture experiments with RAW macrophage cell, the macrophage was stimulated with LPS (10 ng/ml; InvivoGen, tlrl-3pelps) for 10 min and washed with fresh medium, and the separating valve was opened.

Image acquisition

Fluorescence time-lapse images were acquired with complementary metal-oxide semiconductor camera (Hamamatsu, ORCA-Flash4.0 V2) using light-emitting diode (LED) as excitation light source (Lumencor, Spectra X). For the p65-DsRed imaging, cells were imaged with 555-nm excitation with 0.3-s exposure time and 100% LED intensity, while the nucleus marker (H2B-GFP) was captured with 470-nm wavelength and 40-ms exposure time at 100% intensity. All images were acquired with a Nikon S plan Fluor ELWD 20× objective for both fluorescence channel. Images were acquired every 6 min using automated acquisition control by NIS element software (Nikon). Images from each experiment were corrected by subtracting dark frame images and dividing them by the flat field images.

Image and data analysis

With the magnification that we used (×20), each diffusion chamber needed four frames or positions to capture fluorescence images of entire chamber. For each chamber and time point, these images were stitched using custom MATLAB software that used "detectSURFFeatures" and "estimateGeometricTransform" functions to create the transform

matrix. Then, the stitched images were processed through a custom image analysis software (MATLAB) to extract the NF-κB response behavior for each cell in the chamber. Briefly, the software first identified the location and boundary of nucleus through H2B-GFP fluorescence images. Integrating the positions and sizes of nucleus across a sequence of images, the trajectory of each nucleus was evaluated. To sort out the dead or dividing cells, the program also monitors change in the shape or contrast of nucleus and deletes the trajectories that showed any abnormal change in the middle. The selected trajectory and boundary of the nucleus were applied to the corresponding p65-DsRed images to evaluate the NF-κB nucleus translocation, using the similar method as reported in the previous study (*26*). The resulting NF-κB dynamics were smoothed using "lowess" method to reduce the noise from cell migration or collisions between cells. The NF-κB level measured before the start of the experiment (opening of the separating valve) was considered as the basal level for all data in this study. For the analysis that required a number of activated cells in each subregion, two SDs above the mean basal level were used as threshold.

Downstream expression measurement

Cell retrieval process largely followed previously described protocols (*25*). To facilitate the retrieval of cells, the outlet of PDMS chip was cut with razor, so that the purge medium carrying retrieved cells flowed directly onto the glass slide. This allowed cells to settle on the open space in the form of a droplet, which could be retrieved with simple pipetting. After stimulating cells with indicated time, cell chamber was washed and incubated with TryLE express (Gibco) to detach cells from the glass surface for 1 to 2 min. Then, the separating valves were actuated to divide the cell chamber into top, middle, and bottom sections and isolate cells in each position. Each position was then purged with PBS to send detached cells to the outlet. Cells in a ~2-μl droplet were removed and deposited in 10 μl of ice cold lysis buffer containing 0.1% Triton X-100 and ribonuclease inhibitor (Takara). Lysate was stored at −80°C until further processing.

For qPCR, gene-specific reverse transcription and preamplification were performed using the established protocols using a CellDirect One-Step RT-qPCR kit (Thermo Fisher Scientific). Custom primer/probe sets were used to measure the expression of Tnfaip3 (A20), Casp4, and Ccl5 (RANTES), whose sequences are listed in our previous publication (*22*). *CT* values were calculated using software defaults and normalized to glyceraldehyde-3-phosphate dehydrogenase to produce Δ*CT*. The fold change or relative expression level was calculated by comparing Δ*CT* in stimulated samples to unstimulated cells or simply using the following equation, $2^{(\Delta CT\text{unstimulated} - \Delta CT\text{stimulated})}$.

For RNA sequencing, samples were processed through the previously established SMART-Seq2 pipeline with minor variations (*49*). The first-strand synthesis and template switching were performed using SuperScript II (Thermo Fisher Scientific) and a modified template-switching oligo (5′- AAGCAGTGGTATCAACGCAGAGTGAATrGrGrG-3′), which were followed by 10 cycles of preamplification using KAPA HiFi (Roche). The amplified samples were tagmented and indexed (library prep) using Nextera XT reagents (Illumina). The prepped samples were sequenced at the University of Chicago Genomics Facility using Illumina HiSEQ4000 system with a read length of 50 base pairs. Adapter trimming and read mapping were done using STAR with default parameters. Transcript abundance was quantified using featureCounts. Raw counts were normalized, and differentially expressed genes were identified through corresponding R packages, edgeR, and limma. Differential genes between samples were identified using cutoffs false discovery rate < 0.01 and log fold change >1. GO terms and transcription factor motifs were identified using the web tool g:Profiler. NF-κB target genes were identified from genes annotated with a RelA-p65 motif by g:Profiler. Comparison of transcription factor ChIP-seq results was accomplished using the web tool ChEA3 using only ENCODE ChIP-seq data (*39*).

SUPPLEMENTARY MATERIALS

Supplementary material for this article is available at https://science.org/doi/10.1126/sciadv.abn6240

View/request a protocol for this paper from *Bio-protocol*.

REFERENCES AND NOTES

1. A. Hoffmann, D. Baltimore, Circuitry of nuclear factor kappaB signaling. *Immunol. Rev.* **210**, 171–186 (2006).
2. T. Lawrence, The nuclear factor NF-κB pathway in inflammation. *Cold Spring Harb. Perspect. Biol.* **1**, a001651 (2009).
3. S. G. Pereira, F. Oakley, Nuclear factor-κB1: Regulation and function. *Int. J. Biochem. Cell Biol.* **40**, 1425–1430 (2008).
4. Q. J. Cheng, S. Ohta, K. M. Sheu, R. Spreafico, A. Adelaja, B. Taylor, A. Hoffmann, NF-κB dynamics determine the stimulus specificity of epigenomic reprogramming in macrophages. *Science* **372**, 1349–1353 (2021).
5. A. Hoffmann, A. Levchenko, M. L. Scott, D. Baltimore, The IκB-NF-kκB signaling module: Temporal control and selective gene activation. *Science* **298**, 1241–1245 (2002).
6. S. Tay, J. J. Hughey, T. K. Lee, T. Lipniacki, S. R. Quake, M. W. Covert, Single-cell NF-κB dynamics reveal digital activation and analogue information processing. *Nature* **466**, 267–271 (2010).
7. G. Altan-Bonnet, R. Mukherjee, Cytokine-mediated communication: A quantitative appraisal of immune complexity. *Nat. Rev. Immunol.* **19**, 205–217 (2019).
8. G. Voisinne, B. G. Nixon, A. Melbinger, G. Gasteiger, M. Vergassola, G. Altan-Bonnet, T cells integrate local and global cues to discriminate between structurally similar antigens. *Cell Rep.* **11**, 1208–1219 (2015).
9. J. Bagnall, C. Boddington, H. England, R. Brignall, P. Downton, Z. Alsoufi, J. Boyd, W. Rowe, A. Bennett, C. Walker, A. Adamson, N. M. X. Patel, R. O'Cualain, L. Schmidt, D. G. Spiller, D. A. Jackson, W. Müller, M. Muldoon, M. R. H. White, P. Paszek, Quantitative analysis of competitive cytokine signaling predicts tissue thresholds for the propagation of macrophage activation. *Sci. Signal.* **11**, eaaf3998 (2018).
10. R. Cheong, A. Bergmann, S. L. Werner, J. Regal, A. Hoffmann, A. Levchenko, Transient IκB kinase activity mediates temporal NF-κB dynamics in response to a wide range of tumor necrosis factor-α doses. *J. Biol. Chem.* **281**, 2945–2950 (2006).
11. A. Oyler-Yaniv, J. Oyler-Yaniv, B. M. Whitlock, Z. Liu, R. N. Germain, M. Huse, G. Altan-Bonnet, O. Krichevsky, A tunable diffusion-consumption mechanism of cytokine propagation enables plasticity in cell-to-cell communication in the immune system. *Immunity* **46**, 609–620 (2017).
12. L. Chen, H. Deng, H. Cui, J. Fang, Z. Zuo, J. Deng, Y. Li, X. Wang, L. Zhao, Inflammatory responses and inflammation-associated diseases in organs. *Oncotarget* **9**, 7204–7218 (2017).
13. C. A. Thaiss, M. Levy, S. Itav, E. Elinav, Integration of innate immune signaling. *Trends Immunol.* **37**, 84–101 (2016).
14. M. Xu, P. P. Liu, H. Li, Innate immune signaling and its role in metabolic and cardiovascular diseases. *Physiol. Rev.* **99**, 893–948 (2019).
15. Z. Chen, Y. Lu, K. Zhang, Y. Xiao, J. Lu, R. Fan, Multiplexed, sequential secretion analysis of the same single cells reveals distinct effector response dynamics dependent on the initial basal state. *Adv. Sci.* **6**, 1801361 (2019).
16. M. Junkin, A. J. Kaestli, Z. Cheng, C. Jordi, C. Albayrak, A. Hoffmann, S. Tay, High-content quantification of single-cell immune dynamics. *Cell Rep.* **15**, 411–422 (2016).
17. Q. Xue, Y. Lu, M. R. Eisele, E. S. Sulistijo, N. Khan, R. Fan, K. Miller-Jensen, Analysis of single-cell cytokine secretion reveals a role for paracrine signaling in coordinating macrophage responses to TLR4 stimulation. *Sci. Signal.* **8**, ra59 (2015).
18. A. Adamson, C. Boddington, P. Downton, W. Rowe, J. Bagnall, C. Lam, A. Maya-Mendoza, L. Schmidt, C. V. Harper, D. G. Spiller, D. A. Rand, D. A. Jackson, M. R. H. White, P. Paszek, Signal transduction controls heterogeneous NF-κB dynamics and target gene expression through cytokine-specific refractory states. *Nat. Commun.* **7**, 12057 (2016).
19. A. Adelaja, B. Taylor, K. M. Sheu, Y. Liu, S. Luecke, A. Hoffmann, Six distinct NFκB signaling codons convey discrete information to distinguish stimuli and enable appropriate macrophage responses. *Immunity* **54**, 916–930.e7 (2021).

20. R. Cheong, A. Rhee, C. J. Wang, I. Nemenman, A. Levchenko, Information transduction capacity of noisy biochemical signaling networks. *Science* **334**, 354–358 (2011).
21. J. Selimkhanov, B. Taylor, J. Yao, A. Pilko, J. Albeck, A. Hoffmann, L. Tsimring, R. Wollman, Accurate information transmission through dynamic biochemical signaling networks. *Science* **346**, 1370–1373 (2014).
22. M. Son, A. G. Wang, H.-L. Tu, M. O. Metzig, P. Patel, K. Husain, J. Lin, A. Murugan, A. Hoffmann, S. Tay, NF-κB responds to absolute differences in cytokine concentrations. *Sci. Signal.* **14**, eaaz4382 (2021).
23. T. Frank, S. Tay, Automated co-culture system for spatiotemporal analysis of cell-to-cell communication. *Lab Chip* **15**, 2192–2200 (2015).
24. S. Kumar, H. Sharife, T. Kreisel, M. Mogilevsky, L. Bar-Lev, M. Grunewald, E. Aizenshtein, R. Karni, I. Paldor, T. Shlomi, E. Keshet, Intra-tumoral metabolic zonation and resultant phenotypic diversification are dictated by blood vessel proximity. *Cell Metab.* **30**, 201–211.e6 (2019).
25. R. A. Kellogg, R. Gómez-Sjöberg, A. A. Leyrat, S. Tay, High-throughput microfluidic single-cell analysis pipeline for studies of signaling dynamics. *Nat. Protoc.* **9**, 1713–1726 (2014).
26. T. Kudo, S. Jeknić, D. N. Macklin, S. Akhter, J. J. Hughey, S. Regot, M. W. Covert, Live-cell measurements of kinase activity in single cells using translocation reporters. *Nat. Protoc.* **13**, 155–169 (2018).
27. T. K. Lee, E. M. Denny, J. C. Sanghvi, J. E. Gaston, N. D. Maynard, J. J. Hughey, M. W. Covert, A noisy paracrine signal determines the cellular NF-κB response to lipopolysaccharide. *Sci. Signal.* **2**, ra65 (2009).
28. T. Danino, O. Mondragón-Palomino, L. Tsimring, J. Hasty, A synchronized quorum of genetic clocks. *Nature* **463**, 326–330 (2010).
29. T. D. Hassinger, P. B. Guthrie, P. B. Atkinson, M. V. L. Bennett, S. B. Kater, An extracellular signaling component in propagation of astrocytic calcium waves. *Proc. Natl. Acad. Sci. U.S.A.* **93**, 13268–13273 (1996).
30. M. F. Abasıyanık, K. Wolfe, H. Van Phan, J. Lin, B. Laxman, S. R. White, P. A. Verhoef, G. M. Mutlu, B. Patel, S. Tay, Ultrasensitive digital quantification of cytokines and bacteria predicts septic shock outcomes. *Nat. Commun.* **11**, 2607 (2020).
31. P. Rao, M. S. Hayden, M. Long, M. L. Scott, A. P. West, D. Zhang, A. Oeckinghaus, C. Lynch, A. Hoffmann, D. Baltimore, S. Ghosh, IκBβ acts to inhibit and activate gene expression during the inflammatory response. *Nature* **466**, 1115–1119 (2010).
32. M. Baer, A. Dillner, R. C. Schwartz, C. Sedon, S. Nedospasov, P. F. Johnson, Tumor necrosis factor alpha transcription in macrophages is attenuated by an autocrine factor that preferentially induces NF-κB p50. *Mol. Cell. Biol.* **18**, 5678–5689 (1998).
33. M. G. Dorrington, I. D. C. Fraser, NF-κB signaling in macrophages: Dynamics, crosstalk, and signal integration. *Front. Immunol.* **10**, 705 (2019).
34. S. Sen, Z. Cheng, K. M. Sheu, Y. H. Chen, A. Hoffmann, Gene regulatory strategies that decode the duration of NFκB dynamics contribute to LPS- versus TNF-specific gene expression. *Cell Syst.* **10**, 169–182.e5 (2020).
35. S. Anders, D. J. McCarthy, Y. Chen, M. Okoniewski, G. K. Smyth, W. Huber, M. D. Robinson, Count-based differential expression analysis of RNA sequencing data using R and Bioconductor. *Nat. Protoc.* **8**, 1765–1786 (2013).
36. M. D. Robinson, D. J. McCarthy, G. K. Smyth, edgeR: A bioconductor package for differential expression analysis of digital gene expression data. *Bioinformatics* **26**, 139–140 (2010).
37. M. Ashburner, C. A. Ball, J. A. Blake, D. Botstein, H. Butler, J. M. Cherry, A. P. Davis, K. Dolinski, S. S. Dwight, J. T. Eppig, M. A. Harris, D. P. Hill, L. Issel-Tarver, A. Kasarskis, S. Lewis, J. C. Matese, J. E. Richardson, M. Ringwald, G. M. Rubin, G. Sherlock, Gene ontology: Tool for the unification of biology. *Nat. Genet.* **25**, 25–29 (2000).
38. U. Raudvere, L. Kolberg, I. Kuzmin, T. Arak, P. Adler, H. Peterson, J. Vilo, g:Profiler: A web server for functional enrichment analysis and conversions of gene lists (2019 update). *Nucleic Acids Res.* **47**, W191–W198 (2019).
39. A. B. Keenan, D. Torre, A. Lachmann, A. K. Leong, M. L. Wojciechowicz, V. Utti, K. M. Jagodnik, E. Kropiwnicki, Z. Wang, A. Ma'ayan, ChEA3: Transcription factor enrichment analysis by orthogonal omics integration. *Nucleic Acids Res.* **47**, W212–W224 (2019).
40. X. Hu, J. Li, M. Fu, X. Zhao, W. Wang, The JAK/STAT signaling pathway: From bench to clinic. *Sig. Transduct. Target. Ther.* **6**, 402 (2021).
41. M. Iwanaszko, M. Kimmel, NF-κB and IRF pathways: Cross-regulation on target genes promoter level. *BMC Genomics* **16**, 307 (2015).
42. M. Sgarbanti, A. L. Remoli, G. Marsili, B. Ridolfi, A. Borsetti, E. Perrotti, R. Orsatti, R. Ilari, L. Sernicola, E. Stellacci, B. Ensoli, A. Battistini, IRF-1 is required for full NF-κB transcriptional activity at the human immunodeficiency virus type 1 long terminal repeat enhancer. *J. Virol.* **82**, 3632–3641 (2008).
43. H. Iwasaki, J. Mizoguchi, N. Takada, K. Tai, S. Ikegaya, T. Ueda, Correlation between the concentrations of tumor necrosis factor-α and the severity of disease in patients infected with Orientia tsutsugamushi. *Int. J. Infect. Dis.* **14**, e328–e333 (2010).
44. M. Czerkies, Z. Korwek, W. Prus, M. Kochańczyk, J. Jaruszewicz-Błońska, K. Tudelska, S. Błoński, M. Kimmel, A. R. Brasier, T. Lipniacki, Cell fate in antiviral response arises in the crosstalk of IRF, NF-κB and JAK/STAT pathways. *Nat. Commun.* **9**, 493 (2018).
45. D. Rubio, R.-H. Xu, S. Remakus, T. E. Krouse, M. E. Truckenmiller, R. J. Thapa, S. Balachandran, A. Alcamí, C. C. Norbury, L. J. Sigal, Cross-talk between the type 1 interferon and nuclear factor Kappa B pathways confers resistance to a lethal virus infection. *Cell Host Microbe* **13**, 701–710 (2013).
46. T. Kaisho, T. Tanaka, Turning NF-κB and IRFs on and off in DC. *Trends Immunol.* **29**, 329–336 (2008).
47. A. T. Bender, E. Tzvetkov, A. Pereira, Y. Wu, S. Kasar, M. M. Przetak, J. Vlach, T. B. Niewold, M. A. Jensen, S. L. Okitsu, TLR7 and TLR8 differentially activate the IRF and NF-κB pathways in specific cell types to promote inflammation. *ImmunoHorizons* **4**, 93–107 (2020).
48. R. Gómez-Sjöberg, A. A. Leyrat, D. M. Pirone, C. S. Chen, S. R. Quake, Versatile, fully automated, microfluidic cell culture system. *Anal. Chem.* **79**, 8557–8563 (2007).
49. S. Picelli, O. R. Faridani, Å. K. Björklund, G. Winberg, S. Sagasser, R. Sandberg, Full-length RNA-seq from single cells using Smart-seq2. *Nat. Protoc.* **9**, 171–181 (2014).
50. B. Mengel, S. Krishna, M. H. Jensen, A. Trusina, Nested feedback loops in gene regulation. *Phys. A Stat. Mech. Appl.* **391**, 100–106 (2012).
51. S. Krishna, M. H. Jensen, K. Sneppen, Minimal model of spiky oscillations in NF-κB signaling. *Proc. Natl. Acad. Sci. U.S.A.* **103**, 10840–10845 (2006).
52. F. K.-M. Chan, Three is better than one: Pre-ligand receptor assembly in the regulation of TNF receptor signaling. *Cytokine* **37**, 101–107 (2007).
53. M. S. Hayden, S. Ghosh, Regulation of NF-κB by TNF family cytokines. *Semin. Immunol.* **26**, 253–266 (2014).
54. L. Ashall, C. A. Horton, D. E. Nelson, P. Paszek, C. V. Harper, K. Sillitoe, S. Ryan, D. G. Spiller, J. F. Unitt, D. S. Broomhead, D. B. Kell, D. A. Rand, V. Sée, M. R. H. White, Pulsatile stimulation determines timing and specificity of NF-κB-dependent transcription. *Science* **324**, 242–246 (2009).
55. S. L. Werner, J. D. Kearns, V. Zadorozhnaya, C. Lynch, E. O'Dea, M. P. Boldin, A. Ma, D. Baltimore, A. Hoffmann, Encoding NF-κB temporal control in response to TNF: Distinct roles for the negative regulators IκBα and A20. *Genes Dev.* **22**, 2093–2101 (2008).

Acknowledgments

Funding: This work is supported by NIH grants R01GM128042 and R01GM127527 and Army Research Office grant 73231-EL (S.T.). A.T. received funding from the Danish National Research Foundation (grant number: DNRF116). A.G.W. is supported by the NIH MSTP training grant T32GM07281. **Author contributions:** M.S. and T.F. designed and performed the microfluidic experiments with help from M.J., A.G.W., and S.S.K. M.S., T.F., T.H.-H., and A.T. analyzed the data. T.H.-H. and A.T. built the mathematical models and performed the simulations. M.S. and A.G.W. designed and performed the downstream measurements and data analysis. S.T. supervised the work. All authors contributed to writing of the manuscript. **Competing interests:** The authors declare that they have no competing interests. **Data and materials availability:** All data needed to evaluate the conclusions in the paper are present in the paper and/or the Supplementary Materials. RNA sequencing data have been deposited at NCBI Gene Expression Omnibus (GEO) database (GSE189062) and are publicly available as of the date of publication. Single-cell NF-κB dynamics for all experiments and codes for heatmaps and single-cell dynamics have been deposited in Zenodo (DOI: 10.5281/zenodo.6858118) and are publicly available as of the date of publication. The codes for the MDS plot and clustering of RNA sequencing data have been deposited in the same Zenodo repository.

Submitted 9 December 2021
Accepted 19 July 2022
Published 31 August 2022
10.1126/sciadv.abn6240